batteries

Review

Transition Metal Dichalcogenides for High−Performance Aqueous Zinc Ion Batteries

Baishan Liu

CRRC Industrial Academy Co., Ltd., Beijing 100039, China; liubaishan@crrcgc.cc

Abstract: Aqueous zinc ion batteries (ZIBs) with cost—effectiveness, air stability, and remarkable energy density have attracted increasing attention for potential energy storage system applications. The unique electrical properties and competitive layer spacing of transition metal dichalcogenides (TMDs) provide dramatical freedom for facilitating ion diffusion and intercalation, making TMDs suitable for ZIB cathode materials. The recently updated advance of TMDs for high−performance ZIB cathode materials have been summarized in this review. In particular, the key modification strategies of TMDs for realizing the full potential in ZIBs are highlighted. Finally, the insights for further development of TMDs as ZIB cathodes are proposed, to guide the research directions related to the design of aqueous ZIBs while approaching the theoretical performance metrics.

Keywords: aqueous zinc ion batteries; transition metal dichalcogenides; Zn^{2+} diffusion; energy density

check for updates

Citation: Liu, B. Transition Metal Dichalcogenides for High−Performance Aqueous Zinc Ion Batteries. *Batteries* **2022**, *8*, 62. https://doi.org/10.3390/batteries8070062

Academic Editors: Guojin Liang, Funian Mo, Claudio Gerbaldi and Pascal Venet

Received: 16 May 2022
Accepted: 24 June 2022
Published: 29 June 2022

1. Introduction

In order to overcome the energy crisis and environmental degradation in today's society, developing reliable, renewable, and clean energy resources have been considered as a crucial strategy [1]. Lithium ion batteries (LIBs) are the most deeply researched energy storage systems in the commercialized market [2]. However, the widely used organic solvent electrolytes of LIBs may lead to safety concerns and increased costs. Compared with LIBs, aqueous zinc ion batteries (ZIBs) have some advantages, such as cost−effectiveness, air stability, environmental friendliness, and high theoretical energy density, and they have been considered an ideal candidate for next−generation energy devices [3–5]. Thus far, vanadium−based oxides [6], manganese−based oxides [7], and Prussian blue analogs [8] have exhibited remarkable Zn^{2+} storage capabilities, making them suitable for ZIB cathode materials [9]. However, the reversible Zn^{2+} storage behavior exhibited by these materials is not superior enough. For instance, Mn−based or V−based oxides as ZIB cathode materials suffer from poor cycling performance and unsatisfactory conductivity [7]. For Prussian blue analogues, the unstable crystal structure induced phase transformation and limited the capacity [3]. Therefore, exploiting a cathode with a large specific capacity and long−time cycling stability to further increase the Zn^{2+} storage capabilities of ZIBs is highly desired.

Transition metal dichalcogenides (TMDs), such as MoS_2, WSe_2, and VS_2, have been considered as another promising cathode material in energy storage systems, benefitting from unique electrical properties and competitive layer spacing [10]. Compared with the above−mentioned cathode materials, TMDs process the unique hexagonal crystal structure and chemical stability, which may make TMDs exhibit better cycling performance. In particular, the appealing property of TMDs, the wide interlayer distance, is feasible for ion diffusion and intercalation, which is ideal for high−capacity aqueous ZIBs [11]. However, the inserted Zn^{2+}−induced electrostatic interactions and the poor electrical conductivity hinder the capacity of bulk TMDs. As a result, bulk MoS_2 and WS_2 exhibit unsatisfactory capacity of 18 and 22 $mAh \cdot g^{-1}$ as the aqueous ZIB cathode materials, respectively [12]. Hence, efficient strategies for improving the Zn^{2+} storage ability of TMD cathodes are highly desired. In this review, recent advanced approaches to optimize the Zn^{2+} storage ability of TMDs, including interlayer engineering, phase engineering, defect engineering, metallic 1T TMDs, oxidation, and hybridization, have been comprehensively summarized (Scheme 1), which would provide clear guidance to design high−performance TMD−based aqueous ZIBs.

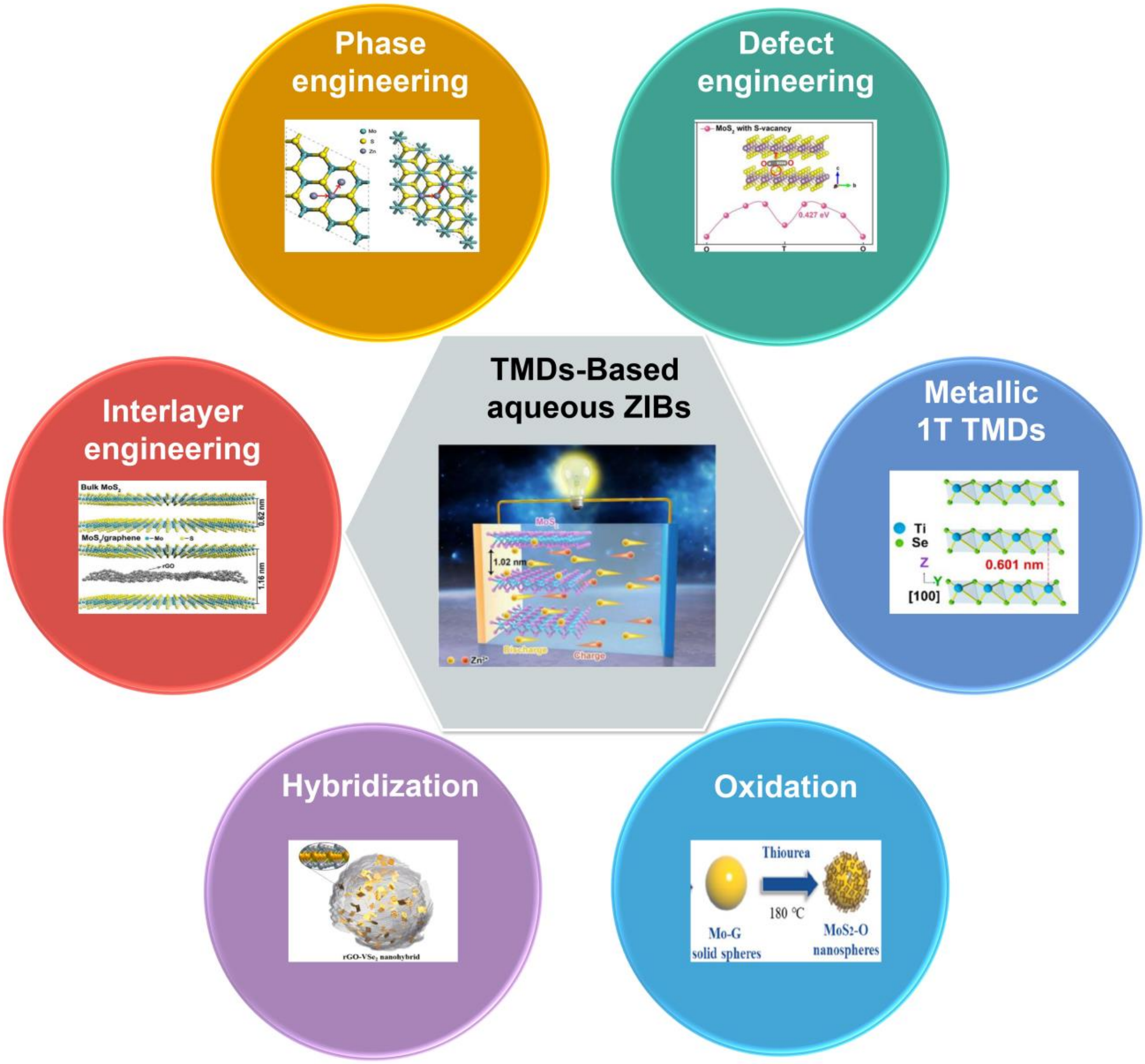

Scheme 1. Schematic of the effective strategies for optimizing the Zn^{2+} storage ability and cycling performance of TMD−based ZIB cathodes. Reprinted with permission from Refs. [13–18]. Copyright 2021, Wiley-VCH GmbH, Weinheim. Copyright 2020, Elsevier. Copyright 2021, Wiley-VCH GmbH, Weinheim. Copyright 2020, Elsevier. Copyright 2021, Elsevier. Copyright 2021, Elsevier.

2. Basic Structural Characteristics of TMDs

These TMDs are a class of materials with the formula MX_2, where M is a transition metal element of group IV, group V or group VI, while X is a brass element. X−M−X is the form of layered TMD materials, in which the brass atoms are located in two hexagonal planes separated by transition metal atoms [19], as shown in Figure 1a,b. In energy−related applications, the most representative TMD is MoS_2.

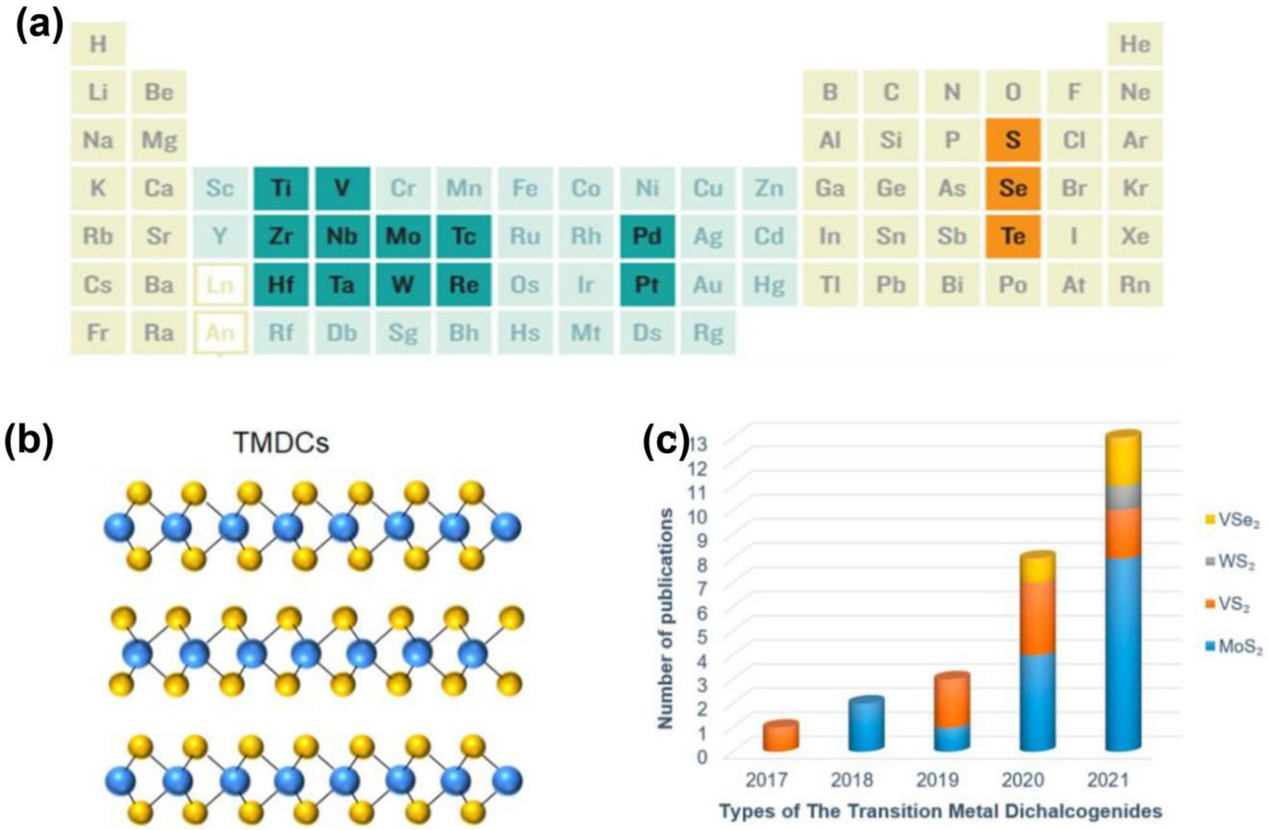

Figure 1. Structure of TMD materials. (**a**) Chemical elements composition of TMD materials. (**b**) Three−dimensional atomic structures of typical TMDs. Reprinted with permission from Ref. [19]. Copyright 2021, Springer. (**c**) The trend of publications on TMDs as ZIB cathode materials. Reprinted with permission from Ref. [10]. Copyright 2022, MDPI (Basel, Switzerland).

The bulk MoS_2 usually consists of monolayer MoS_2 van der Waals stacked together. MoS_2 is the extensively researched electronic material for various energy−related devices. In general, MoS_2 has three different crystalline phases: 2H (hexagonal symmetry), 3R (rhombohedral symmetry) and 1T (tetragonal symmetry) [20]. For different phases, the arrangement of MoS_2 monolayers is different, which may lead to different physical and chemical properties and which may provide flexibility for material design. More importantly, due to the large interlayer spacing (0.62 nm), TMDs can ensure the diffusion of a larger radius of cations favorable as ZIB cathode materials. The year−on−year increase in the number of published articles is evidence of the growing interest in TMD materials for ZIBs (Figure 1c) [10].

3. Proposed Modifying Strategies for the TMDs Cathode of Aqueous ZIBs

In general, the specific capacity of pristine MoS_2 as the ZIB cathode is about 1–40 mAh·g^{-1} [12]. In order to accommodate hydrated Zn^{2+}, the host material must embrace a layer spacing larger than its radius (0.40–0.43 nm). Although the layer spacing of bulk MoS_2 (≈0.62 nm) is larger than the radius of hydrated Zn ions, the poor electrochemical activity and low electrical conductivity of intrinsic MoS_2 are not feasible for reversible intercalation of Zn^{2+}. When pristine MoS_2 and WS_2 obtained in nature were tested in aqueous $ZnSO_4$ solutions, no observable redox peaks were observed, suggesting that the intrinsic MoS_2 and WS_2 cannot store reasonable amounts of Zn^{2+} to show acceptable capacity [12].

Based on the above discussion, modification strategies become important in order to obtain outstanding performance from TMDs for functional ZIB cathodes. In this section, six effective methods to overcome the high Zn^{2+} intercalation energy barriers of TMDs and to ensure the structural stability of TMDs are proposed: (1) interlayer engineering, (2) phase engineering, (3) defect engineering, (4) metallic 1T TMDs, (5) oxidation, and (6) hybridization.

3.1. Interlayer Engineering

The intercalation of small guest layers, such as ions and molecules, can tune the interlayer spacing of TMDs due to the unique van der Waals stacking. Therefore, interlayer engineering is a widely used means to modulate the electrochemical properties of TMDs. Via interlayer engineering, TMDs can not only achieve larger interlayer spacing but can also obtain more stable structures. Meanwhile, the energy barrier of Zn^{2+} intercalation can be lowered, and the storage of Zn^{2+} can also be enhanced in the TMDs framework with larger interlayer spacing. Furthermore, the interlayer engineering becomes more critical if the diffused hydrated Zn^{2+} is to be separated through a narrow gap in MoS_2. As the layer spacing of MoS_2 increases, the effective energies can be lowered at similar hydration levels [21]. Based on these benefits, there are many researchers exploiting the various intercalators to modify the MoS_2 interlayer spacing to functionalize the ZIBs.

Zhang et al. synthesized MoS_2-nH_2O nanoflowers for storing Zn^{2+} via hydrothermal synthesis [22], and the layer spacing of MoS_2 can be enlarged by water (Figure 2a). In addition, the electrostatic interaction between Zn^{2+} and the host material can be shielded, which further increases the Zn^{2+} diffusion channel. MoS_2-nH_2O exhibited a high reversible capacity of 165 $mAh{\cdot}g^{-1}$ at 0.1 $A{\cdot}g^{-1}$ (Figure 2b,c). The capacity retention was 88% after 800 cycles at 2 $A{\cdot}g^{-1}$. Moreover, the insertion of highly conductive carbon material between MoS_2 layers is another approach often used in interlayer engineering [13,15,23]. The synergistic effect of expanding the layer spacing and enhancing the conductivity can effectively improve the performance of MoS_2−based ZIBs. Liu et al. [13] used an electrostatic self−assembly strategy to successfully insert graphene between molybdenum disulfide layers, leading to the enlarged layer spacing from 0.62 to 1.16 nm (Figure 2d), and the reduced graphene oxide and 1T−rich phase MoS_2 gave the material better ionic/electronic conductivity. The "sandwich" structure of MoS_2/graphene composite nanosheets self−assembled into a nanoflower structure can effectively suppress the stacking of molybdenum disulfide and graphene layers, which is conducive to sufficient electrolyte infiltration and rapid diffusion of zinc ions to maintain structural stability. Compared with bulk molybdenum disulfide (21.9 $mAh{\cdot}g^{-1}$ at 0.05 $A{\cdot}g^{-1}$), the material has more than 10 times higher zinc storage capacity (285.4 and 141.6 $mAh{\cdot}g^{-1}$ at 0.05 and 5 $A{\cdot}g^{-1}$, respectively) and remarkable cycling stability, as displayed in Figure 2e. Except for the interlayer engineering, the highly flexible and reversible transition of MoS_2 between the 2H−phase and 1T−phase during Zn^{2+} insertion/extraction also contributed to the remarkable storage capacity. The cycling stability is remarkable (about 88.2% capacity retention after 1800 cycles), which benefits from the large spacing−induced low Zn ion migration barriers that are also verified by density function theory calculation (Figure 2f). By combining interlayer polymerization with template−assisted insertion of N−doped carbon between MoS_2 layers, Li et al. produced MoS_2 nanocages with multilevel structures with expanded interlayer spacing, as displayed in Figure 2g [23]. The cage structure suppresses the accumulation of nanosheets. Meanwhile, the ion migration induces the volume expansion of alleviates during (non)charging. As a result, the layer spacing−enhanced MoS_2 exhibits high zinc storage capacity (247.8 $mAh{\cdot}g^{-1}$ at 0.1 $A{\cdot}g^{-1}$) and remarkable capacity retention (85.6% after 3200 cycles at 1.0 A g^{-1}) (Figure 2h).

3.2. Phase Engineering

Phase engineering has been verified as a potential technique to tune the electrochemical properties of materials [24]. Monolayer TMDs can exist in three different types according to the atomic configuration, namely 1T, 2H, and 3R. Monolayer TMDs can be composed of either a trigonal phase (2H) or an octahedral phase (1T). Phase control may be key to the electronic properties modification of TMDs. This is because the TMD phase is strongly related to the electron d−orbital density of the transition metal. When the Zn diffusion pathway was simulated, 2H MoS_2 exhibits a higher Zn energy barrier than 1T MoS_2, regardless of the interlayer spacing [14], indicating that the reversible Zn^{2+} storage can be effectively activated via phase control. Interleaving alkaline metals is the most common method for controlling TMDs phase transitions. Taking Li ion batteries as an example, electrons are transferred to the TMD via the insertion of an alkaline metal, leading to an increase in the d−orbital electron density. As a result, the phase transition of TMDs from 2H to 1T can be accomplished through increasing the d−orbital electron density [25]. Lithium−containing compounds, such as n−butyllithium diluted in hexane, were used to achieve the phase transition of TMDs [26]. Furthermore, 1T MoS_2 with increased interlayer spacing can be obtained by intercalation of Na^+ into 2H MoS_2 as demonstrated by Zeng et al. Therefore, alkali metal intercalation−induced phase transition of TMDs has been verified as a synergistic method to activate MoS_2 and TMDs for Zn^{2+} storage [27].

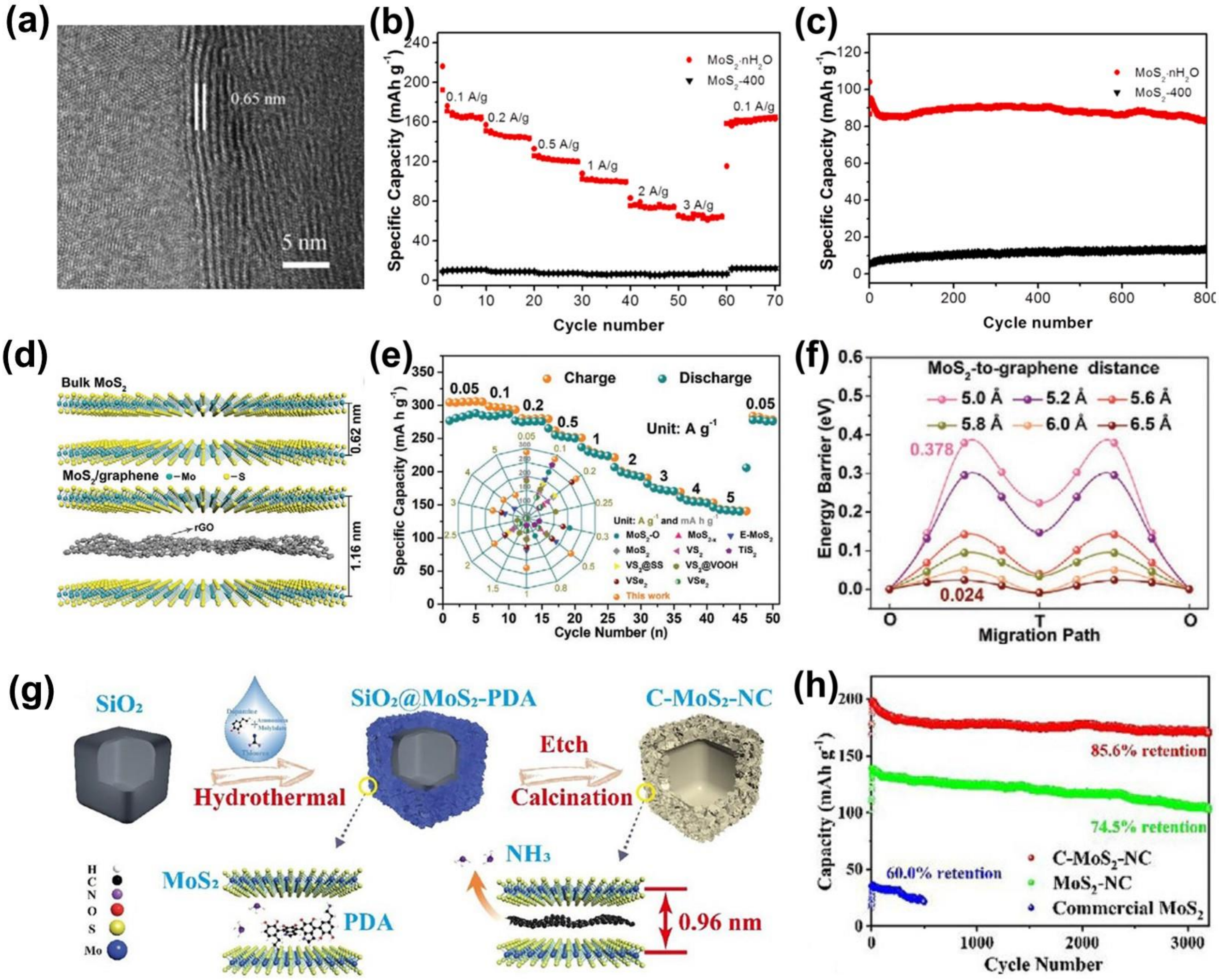

Figure 2. Interlayer engineering for optimized MoS_2−based ZIBs. (**a**) HRTEM images of $MoS_2{\cdot}nH_2O$. (**b**) Rate performance of Zn/$MoS_2{\cdot}nH_2O$ and Zn/MoS_2−400 battery at 2 $A{\cdot}g^{-1}$. Reprinted with permission from Ref. [22]. Copyright 2021, Elsevier. (**c**) Cycling performance of Zn/$MoS_2{\cdot}nH_2O$ and Zn/MoS_2−400 battery. (**d**) Crystal structures of bulk MoS_2 and graphene−enlarged MoS_2. (**e**) Rate capability of the graphene−enlarged MoS_2 at 0.05−5 $A{\cdot}g^{-1}$. (**f**) Migration barriers associated with MoS_2 and graphene distances. Reprinted with permission from Ref. [13]. Reprinted with permission from Ref.Copyright 2021, Wiley-VCH GmbH, Weinheim. (**g**) Illustration of the synthetic process of C−MoS_2−NC. (**h**) The capacity retention performance comparison for the various MoS_2 cathodes. Reprinted with permission from Ref. [23]. Copyright 2022, Elsevier.

For the first time, Liu et al. prepared defective MoS_2 with different phases as ZIB cathode materials (Figure 3a). $1T-MoS_2$ performed more remarkable specific capacity and more remarkable capacity retention than $2H-MoS_2$ in aqueous ZIBs. The combination of experiments and DFT calculations reveals that $1T-MoS_2$ can effectively lower the Zn^{2+} diffusion energy barrier (Figure 3b). Tang et al. demonstrated that $1T-WS_2$ nanosheets obtained via phase engineering can be used as a ZIB cathode candidate. Benefiting from the interlayer expanding (Figure 3c) and conductivity increasing of the 1T phase, the reversible discharge capacities of the synthesized WS_2-200 at current densities of 50, 100 and 200 mA·g^{-1} were 233.26, 206.25 and 179.99 mAh·g^{-1}, respectively, with 179.99 mAh·g^{-1} far exceeding the discharge capacity of the commercial $2H-WS_2$ (22 mAh·g^{-1} at 200 mA·g^{-1}), as displayed in Figure 3d.

To further enhance the transfer kinetics of zinc ions, the vertically aligned 1T phase MoS_2 was fabricated by Liu et al., as displayed in Figure 3e [28]. The vertically aligned freestanding structure of the $1T-MoS_2$ contributed to a remarkable specific capacity of 198 mA h·g^{-1} at 0.1 A·g^{-1} (Figure 3f). More importantly, it also exhibits remarkable cycling stability with a specific capacity retention of 97.2% after 1000 cycles at a current density of 2 A·g^{-1} (Figure 3g).

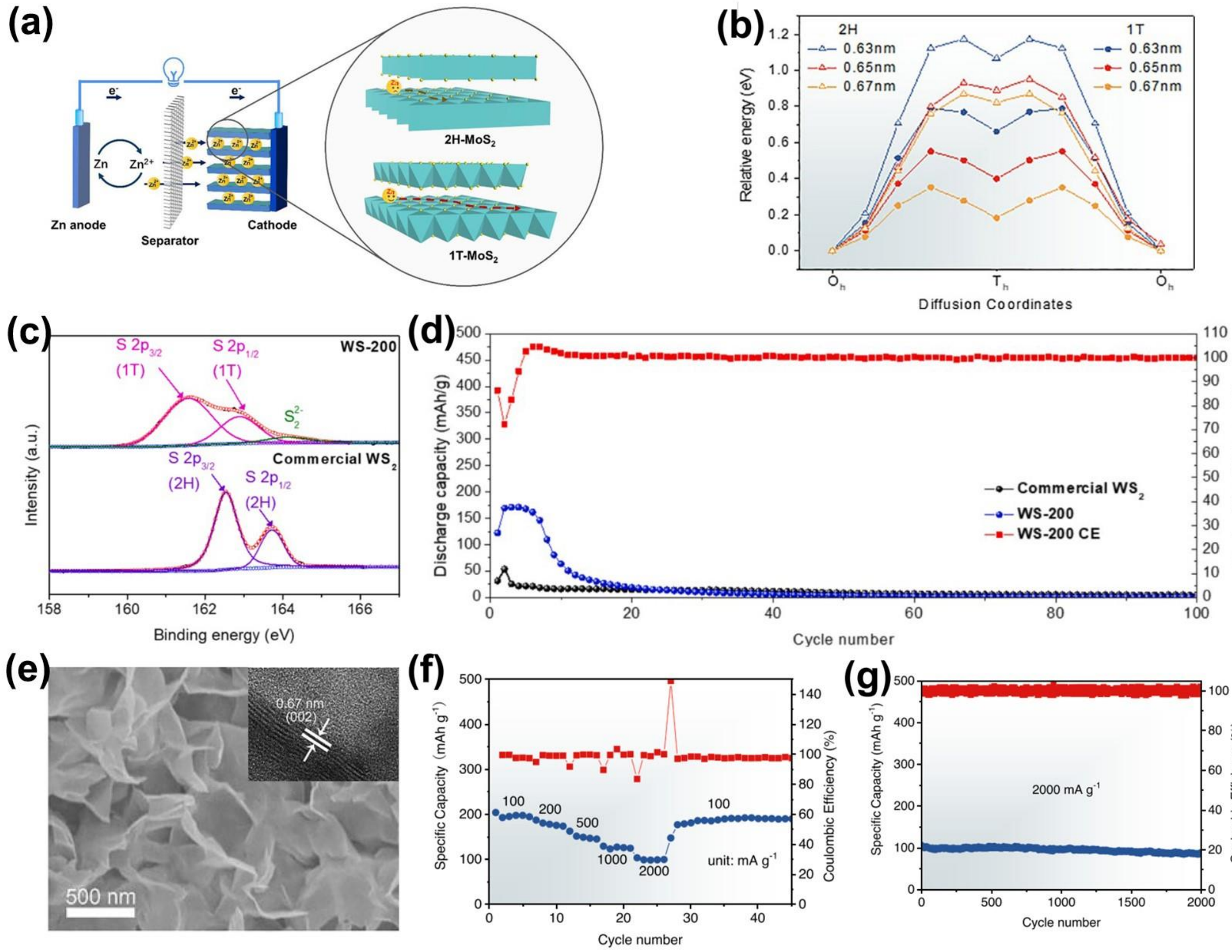

Figure 3. Phase−engineered TMDs for ZIB cathode. (**a**) Illustration of the rechargeable Zn/MoS_2 battery system. (**b**) Relative Zn^{2+} diffusion energies associated with the interlayer spacing in 2H and 1T MoS_2. Reprinted with permission from Ref. [14]. Copyright 2020, Elsevier. (**c**) High−resolution XPS spectra of S_{2p} in the commercial WS_2 and WS_2-200 ($1T-WS_2$) samples. (**d**) Galvanostatic charge/discharge curves of WS_2-200 with various current densities. Reprinted with permission from

Ref. [29]. Copyright 2022, Elsevier. (**e**) SEM images of vertically aligned $1T-MoS_2$. Inset: Section TEM images of $1T-MoS_2$. (**f**) Specific capacity of $1T-MoS_2$ from 0.1 to 2 $A \cdot g^{-1}$. (**g**) Capacity retention of $1T-MoS_2$ at $2A \cdot g^{-1}$. Reprinted with permission from Ref. [28]. Copyright 2022, Elsevier.

3.3. Defect Engineering

Defect engineering is another widely studied method to change the physical and chemical properties of TMDs [15,30–33]. Defect engineering causes structural changes in TMDs, which facilitate the optimization of Zn^{2+} ion diffusion and charge transfer processes [34]. In addition, defect engineering can increase the number of ion storage sites and can achieve higher charge capacity. Defect engineering has been verified by many studies that can help improve the kinetics of reactions and electrochemical properties due to the active sites increasing [35]. Therefore, the implementation of defect engineering in TMDs is a feasible approach to tuning electrochemical properties for functional cathodes.

Vacancy is one of the most common structural defect of materials, such as sulfur vacancies, transition metal vacancies, edges, and holes in TMDs lattice, as shown in Figure 4a [34,36]. These vacancy defects are particularly attractive in two−dimensional monolayer TMDs because the transport of charge carriers in the two−dimensional plane is significantly enhanced. Moreover, the creation of vacancies exposes sites in the TMDs that can then be used for chemical functionalization [37,38]. It has been reported by Liu et al. that the formation energy of S vacancies in MoS_2 (2.35 eV) is lower than that of Mo vacancies (8.02 eV) [39], indicating that it is easier to generate S vacancies than Mo vacancies, which is also verified by Koh et al. [40]. In particular, S vacancy is critical for the storage mechanism due to the ability to facilitate ion transit through the MoS_2 layer [41]. Xu et al. investigated defect−engineered MoS_{2-x} nanosheets as cathodes for zinc ion batteries [42]. Compared with defect−free MoS_2, the defect−rich MoS_{2-x} nanosheets provided more intercalation sites for zinc ions, resulting in higher capacity (Figure 4b). More importantly, it also exhibits remarkable cycling stability with a specific capacity retention of 87.8% after 1000 cycles at a current density of 1 $A \cdot g^{-1}$ (Figure 4c).

Recently, Liu et al. successfully unlocked the molybdenum disulfide substrate by implanting structural defects and lattice oxygen ($D-MoS_2-O$) in molybdenum disulfide through in situ molecular engineering (Figure 4d) [15], expanding the layer spacing from 6.2 to 9.6 Å. The enriched 1T phase gives the material better electrical conductivity and hydrophilicity and achieves efficient three−dimensional transport of zinc ions along the ab−plane and c−axis of molybdenum disulfide. The prepared molybdenum disulfide nanosheets containing structural defects and lattice oxygen are grown vertically on a carbon cloth substrate, which effectively suppresses the stacking of molybdenum disulfide layers and facilitates sufficient electrolyte infiltration and rapid diffusion of zinc ions. Benefiting from the synergistic engineering (structural defects and 1T−phase transition) that induces interlayer expanding, the material exhibits remarkable multiplicative performance (reversible capacities of 261 and 102.4 $mAh \cdot g^{-1}$ at 0.1 and 10 $A \cdot g^{-1}$, respectively) and outstanding cycling stability (90.5% capacity retention after 1000 cycles). Electrochemical tests of the system indicate that the material has a high zinc ion diffusion coefficient, while DFT theoretical calculations demonstrate a low Zn^{2+} migration energy barrier and a feasible three−dimensional zinc ion transport mechanism in the material (Figure 4e).

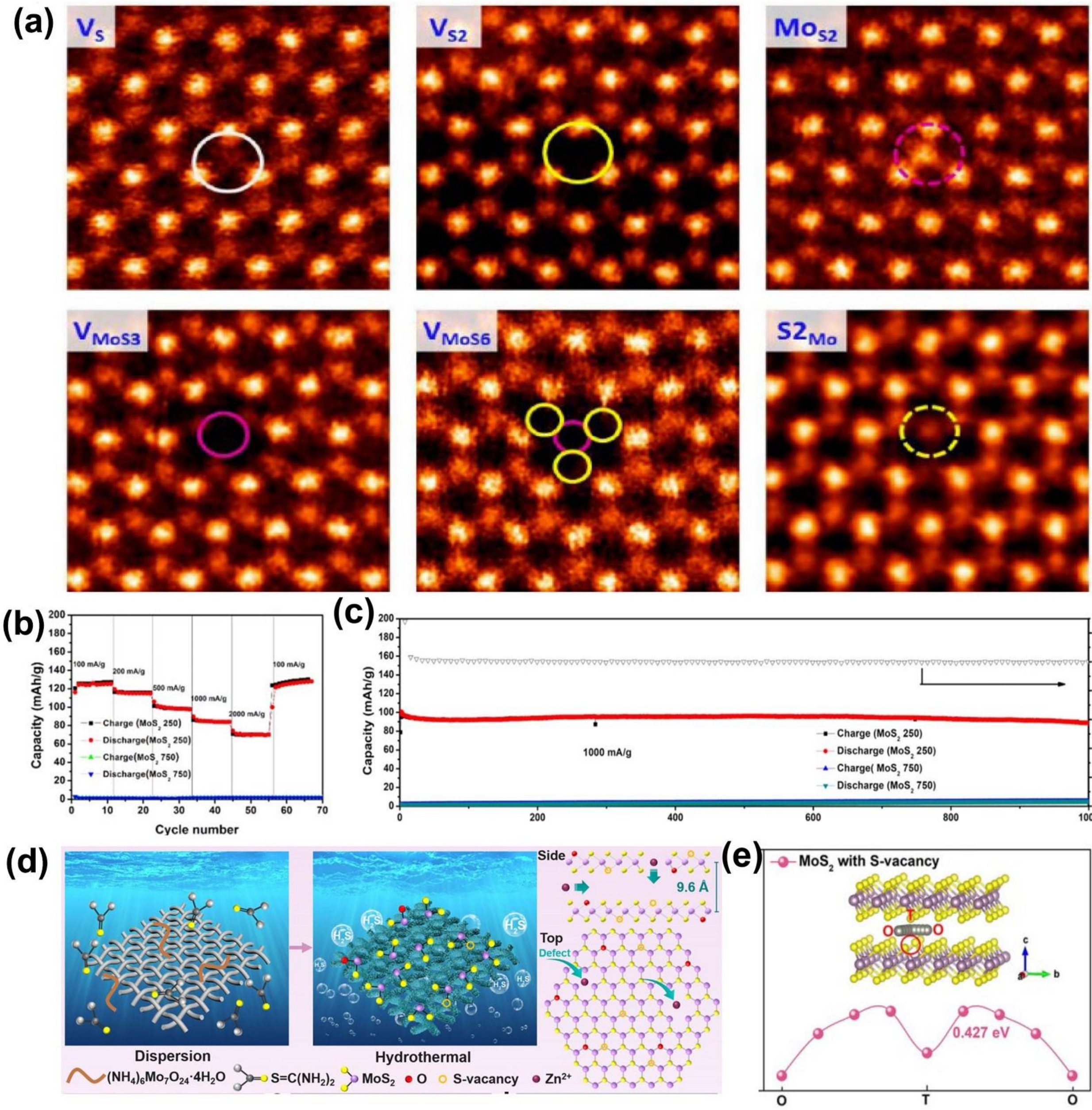

Figure 4. Defect−tailored MoS_2 for ZIB cathode. (**a**) Characterization of various point defects in single−layer MoS_2, including V_S, V_{S2}, Mo_{S2}, V_{MoS3}, V_{MoS6}, and $S2_{Mo}$. Reprinted with permission from Ref. [34]. Copyright 2013, American Chemical Society. (**b**) Rate performance of defect−rich MoS_{2-x} at various currents densities. (**c**) Long−term cyclic properties of MoS_{2-x} at specific current of 1 $A{\cdot}g^{-1}$. Reprinted with permission from Ref. [42]. Copyright 2019, Elsevier. (**d**) Illustration of the preparation process and the crystal structure of defect−engineered MoS_2−O. (**e**) Zn ion migration behaviors along the ab plane in O−doped MoS_2 with S−vacancy. Reprinted with permission from Ref. [15]. Copyright 2021, Wiley-VCH GmbH, Weinheim.

3.4. Metallic 1T TMDs

Beyond the 1T phase transition of 2H MoS_2 and WS_2, the direct selection of metallic 1T phase TMDs is another effective strategy to ensure large layer spacing and high electric conductivity, while the structure is also more easily stabilized compared to that of 1T−MoS_2/WS_2 during the phase transition process.

Li et al. developed metallic 1T− VS_2 directly grown on stainless steel (VS_2@SS) mesh cathode for an aqueous ZIB [43]. The cell exhibited a remarkable Zn ion storage capacity

(198 mAh·g^{-1}) and stable cycling performance (more than 80% capacity retention over 2000 cycles at 2 A·g^{-1}), which suggests that the electrode is promising for practical applications. Wu et al. observed the remarkable zinc ion storage properties in ultrathin VSe_2 nanosheets (Figure 5a) [44]. The X−ray photoelectron spectrum (XPS) unveiled the two−step intercalation/de−intercalation reaction mechanism of VSe_2 (Figure 5b). VSe_2 nanosheets exhibited a specific capacity of 131.8 mAh·g^{-1} at 0.1 A·g^{-1} and a high energy density of 107.3 Wh·kg^{-1} (power density of 81.2 W·kg^{-1}). Moreover, the ZIBs with this material exhibit remarkable cycling stability (80.8% capacity retention after 500 cycles) (Figure 5c).

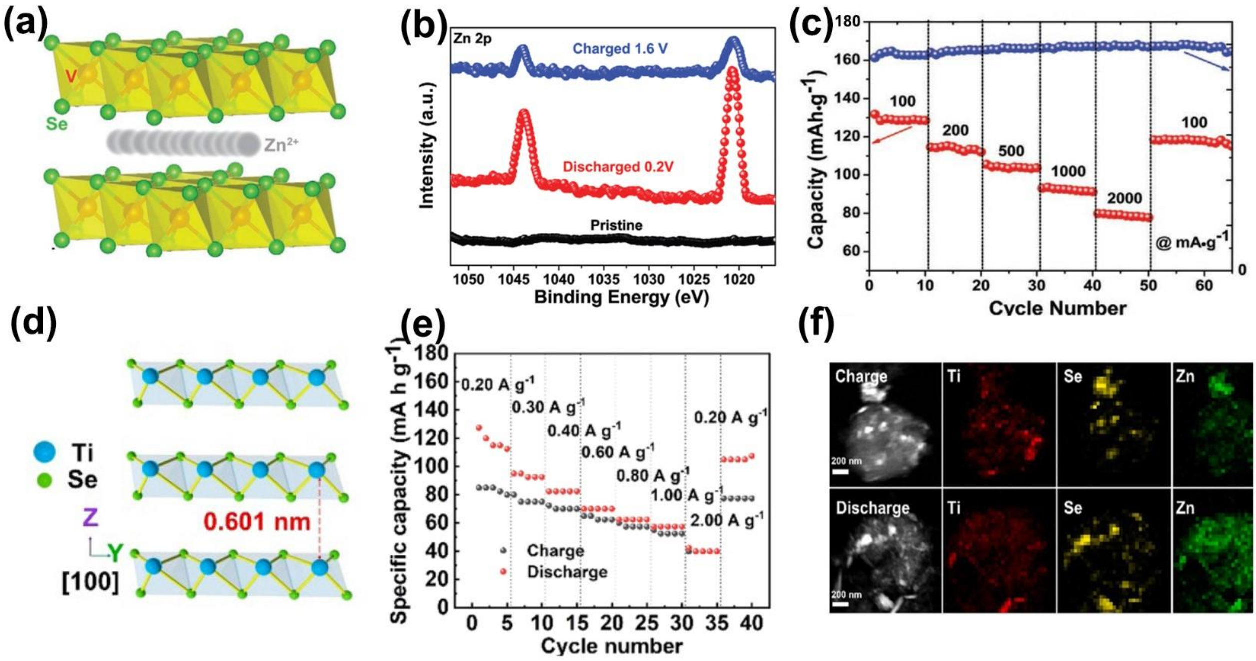

Figure 5. Metallic 1T TMDs for high−performance ZIBs. (**a**) Atomic structure of VSe_2. (**b**) Ex situ high−resolution XPS of the Zn 2p of the cathode at different states. (**c**) Rate performance of VSe_2 electrodes from 0.10 to 2.00 A·g^{-1}. Reprinted with permission from Ref. [44]. Copyright 2020, Wiley-VCH GmbH, Weinheim. (**d**) Schematic atomic structure of $TiSe_2$. (**e**) Rate capability at various current densities. (**f**) Elemental distribution characterization of discharged/charged $TiSe_2$. Reprinted with permission from Ref. [16]. Copyright 2021, Elsevier.

Recently, $TiSe_2$ was verified to be an ideal candidate for aqueous ZIBs by Wen et al., as shown in Figure 5d [16]. The $TiSe_2$ with 0.601 nm layer spacing and good electron conduction properties make it suitable for efficient (de)intercalation of zinc ions. As a result, the $TiSe_2$ electrode showed a capacity of 128.0 mAh·g^{-1} at 0.20 A·g^{-1} (Figure 5e) and recoverability of 70.0% after 300 cycles. Especially, the high concentration distribution of zinc ions in the fully discharged state demonstrates the accomplished intercalation of zinc ions (Figure 5f).

3.5. Oxidation

The use of in situ electrochemistry to oxidize the inserted ions to the corresponding oxides without changing the ion insertion position of the TMD, not only increases the active site but also enhances the hydrophilicity of the ions, leading to an effective diffusion of Zn^{2+} [45,46].

To verify the effectiveness of in situ oxidation, Yu et al. constructed VS_2/VOx composite structures with porous VO_x nanosheets uniformly distributed on VS_2 using electrochemical pretreatment [47]. In particular, the lattice fringes of 0.295 and 0.345 nm correspond to the (400) and (100) planes of V_6O_{13} (Figure 6a). Benefiting from the synergy of the high conductivity of VS_2 and the remarkable stability of VO_x, the VS_2/VO_x heterostructure facilitates the regulation of guest ion intercalation and improves the chemical stability of the VS_2 backbone. The buffer volume was changed by the gradual insertion of Zn^{2+} while accelerating the reversible reaction kinetics. The VS_2/VO_x electrode maintained a high capacity of 75% after 3000 cycles at 1 $A{\cdot}g^{-1}$. (Figure 6b). In addition, MoS_2−O was prepared as a cathode for ZIBs by a simple solvothermal method by Jia et al. [17]. EDS and XPS characterization verifies the existence of O insertion in MoS_2 (Figure 6c,d). MoS_2−O reduced the ion diffusion resistance and maintained the stability of the MoS_2 layer. The optimized MoS_2−O electrode exhibited a high specific capacity of 206.7 $mAh{\cdot}g^{-1}$ at a current density of 0.1 $A{\cdot}g^{-1}$ (Figure 6e) and remarkable cycling stability after 300 cycles, further confirming the effectiveness of the oxidation strategy.

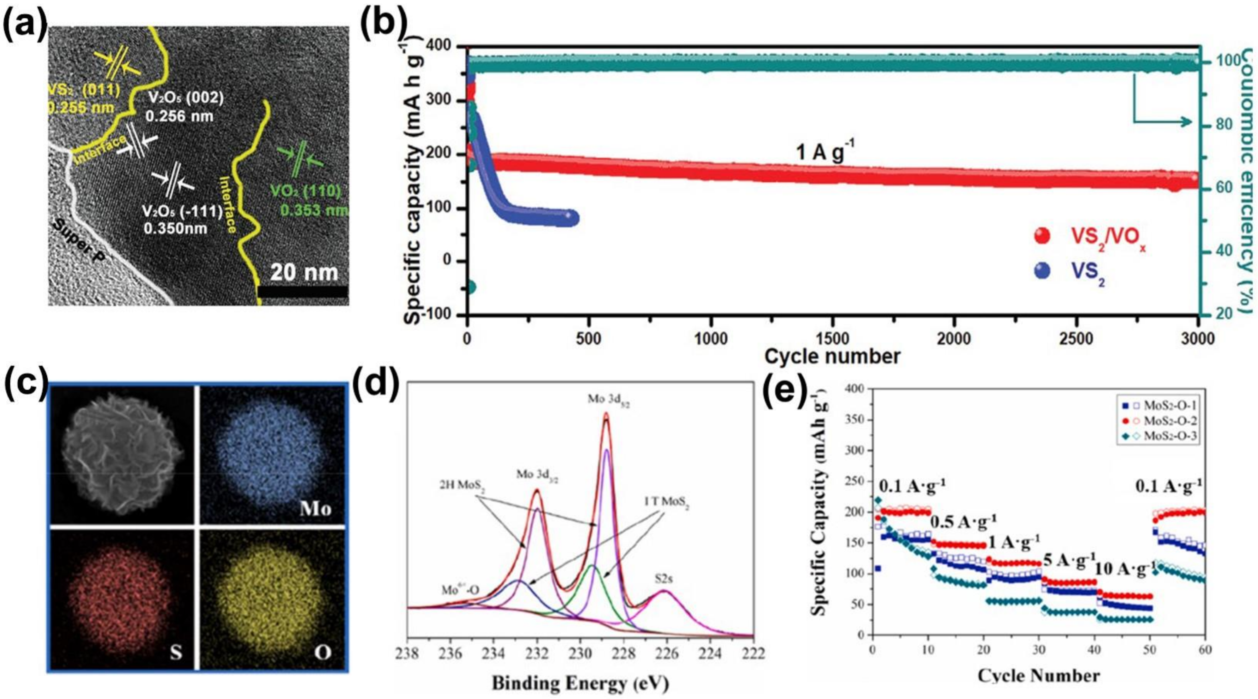

Figure 6. Modification of TMD−based ZIBs by electrochemical oxidation. (**a**) The TEM image of in situ formed VS_2/VO_x. (**b**) The cycling performance of VS_2/VO_x heterostructure at 1 $A{\cdot}g^{-1}$. Reprinted with permission from Ref. [47]. Copyright 2021, Wiley-VCH GmbH, Weinheim. (**c**) Elemental characterization in MoS_2−O. (**d**) XPS survey spectra of MoS_2−O. (**e**) Rate performance of MoS_2−O at various current densities. Reprinted with permission from Ref. [17]. Copyright 2021, Elsevier.

3.6. Hybridization

Hybridization is another well−proven method for altering the properties of a material or for giving it new properties [48]. Two−dimensional TMDs can be compounded with other materials to obtain new properties. In general, DMTs have low electrical conductivity, which can considerably limit the specific capacity that they can achieve. To overcome the challenge, the researchers demonstrated that the electrochemical properties of the entire composite can be improved via hybridizing the host TMDs with other materials, such as other TMDs, carbon materials, and so on [49].

The hybridization strategy is particularly applicable between TMD materials because the host and guest TMDs usually have similar structures and the lattice mismatch can be neglected. Generally, the host and guest TMDs can be hybridized by epitaxial growth, and the composites are often able to exhibit stronger intrinsic properties, multifunctionality, or even new properties. For example, a MoS_2−$MoSe_2$ heterostructure assembled by liquid−phase ultrasound−assisted exfoliation was reported by Yang et al. [50]. Benefiting from the unique van der Waals interlayer coupling, the MoS_2−$MoSe_2$ heterostructure is able to provide more electrochemical active sites. Moreover, the fluffy construction of the

MoS_2−$MoSe_2$ heterostructure enhances ion transport. Pu et al. fabricated VS_2@VOOH via hydrothermal synthesis (Figure 7a) [51]. The presence of V−O−V and O−H vibrational was demonstrated by FT−IR spectroscopic characterization at typical 480 and 1610 cm^{-1} adsorption peaks, respectively (Figure 7b), which further solidifies the existence of VOOH in VS_2. The O−H in VOOH not only improved the wettability of the electrode and electrolyte, but also reduced vanadium dissolution and improved the electrochemical performance. This composite displayed a remarkable capacity of 107.5 mAh·g^{-1} after 350 cycles at 1.5 A·g^{-1}. In particular, after 400 cycles at a high current density of 2.5 A·g^{-1}, it maintains a capacity of 91.4 mAh·g^{-1} (Figure 7c). In the hybridization of cathode materials for energy storage systems, both carbon nanotubes and graphene are widely used for their remarkable electrical and mechanical properties [52,53], and by hybridizing TMDs and CNT/graphene, the conductivity of the whole composite can be effectively improved while maintaining a large layer spacing colleague. A novel two−dimensional layered composite composed of graphene sheets were grown vertically on metallic 1T−VS_2 nanosheets by a one−step solvothermal strategy by Chen et al. [54], as shown in Figure 7d. The rGO−VS_2 was confirmed by Raman spectroscopy (Figure 7e). Due to the advantageous synergy between the layered VS_2 and graphene nanosheets, the rGO−VS_2 composites demonstrated a high capacity of 238 mAh·g^{-1} at 0.1 A·g^{-1} and capacity retention of more than 93% after 1000 cycles at 5 A·g^{-1} as ZIB cathodes (Figure 7f).

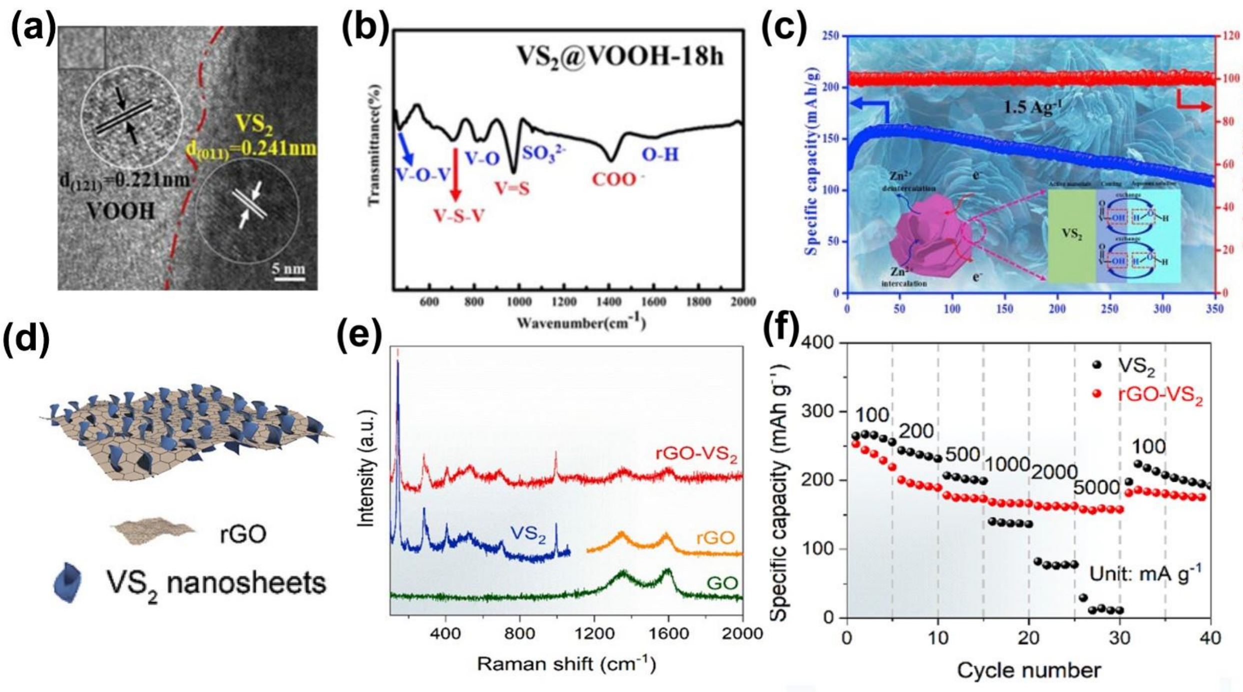

Figure 7. Hybridization of TMDs for high−performance ZIBs. (**a**) HRTEM images of the VS_2@VOOH. (**b**) FTIR spectra of VS_2@VOOH. (**c**) Cycling retention at 1.5 A·g^{-1} of VS_2@VOOH. Reprinted with permission from Ref. [51]. Copyright 2019, Elsevier. (**d**) Illustration of hierarchical rGO−VS_2 composites. (**e**) Raman characterization of the GO, rGO, VS_2, and rGO−VS_2. (**f**) Rate capability of rGO−VS_2 and VS_2 Reprinted with permission from Ref. [54]. Copyright 2020, Elsevier.

Yan et al. synthesized marble−like rGO−VSe_2 nanobridges [18]. Benefiting from the inhibition of electrostatic buildup of VSe_2 nanosheets by the strongly conducting rGO, the electrolyte diffusion path is shortened, while the highly conductive rGO network provided a three−dimensional highway for electron transport and improved reaction kinetics. The rGO−VSe_2 nanohybrids were used as the ZIB cathode candidate, exhibiting high capacity 221.5 mAh·g^{-1} at a current density of 0.5 A·g^{-1}, and performed 91.6% capacity retention after 150 cycles. Wang et al. combined metal 1T phase MoS_2 with multi−walled carbon nanotubes (MWCNT) to construct ZIB cathode materials by the hydrothermal method [55]. The synergistic effect of phase engineering and hybridization was utilized to accelerate the zinc ion transfer kinetics and to cost−effectively improve electrochemical properties at room temperature and low temperature. The hybrid electrode exhibited a high reversible capacity of 161.5 $mAh \cdot g^{-1}$ with good cycling stability after 100 cycles at 0.1 $A \cdot g^{-1}$ and capacity retention of 84.6% after 500 cycles at 1 $A \cdot g^{-1}$.

4. Conclusions and Perspective

In this review, potential ZIB cathode materials, TMDs, are systematically discussed. The timeline and electrochemical performance of TMD materials as ZIB cathode is summarized in Figure 8 and Table 1. In order to effectively reduce the diffusion potential of Zn^{2+} in TMDs and maintain the stability of the material over multiple cycles, six possible strategies for eliciting satisfactory electrochemical performance of TMDs, including (1) interlayer engineering, (2) phase engineering, (3) defect engineering, (4) metallic 1T TMDs, (5) oxidation, and (6) hybridization are comprehensively summarized in this review. Although these modification strategies have only been initially validated in some TMD materials, more members of the TMDs family will definitely become excellent ZIB cathode materials as the research continues, driving the flourishing development of aqueous ZIBs. To further the continuous upgrade of these modification strategies, we also conclude by listing a few key breakthrough directions:

(1) Focusing on mechanism exploration behind the ZIBs technology:

Although previous studies have analyzed the electrochemical properties of TMD−based ZIBs and their energy storage mechanisms, the link between the lattice structure, crystal defects and properties of cathode materials needs to be deeply resolved. Fully revealing the effects of various strategies, engineered TMDs on Zn^{2+} storage behavior is crucial to achieving higher performance ZIB batteries.

(2) Increasing synergistic engineering between different strategies:

Each of the strategies mentioned above addresses a specific performance enhancement of TMD−based ZIBs. To achieve the overall enhancement, the interplay between different modified strategies is required, such as the synergy of defect engineering and phase engineering increasing the layer spacing [15], reducing the Zn^{2+} transport barriers, and enhancing the cycling characteristics. The hybridization of metallic 1T−TMD materials and graphene enhances the stability of the material while guaranteeing conductivity. More strategy combinations provide new freedom to design high−performance ZIBs.

(3) Solving cyclic stability from a system perspective:

In ZIBs, the storage capacity can approach theoretical values by material selection and modifications. However, the storage capacity suffers from rapid fading upon long−term cycling, which is more crucial for the commercialization of ZIBs. For TMD−based ZIBs, improving material structure and chemical stability are the basic guarantees. In addition, in−depth exploration of the underlying and overall correlation between TMD cathode materials, electrolytes, and Zn anodes is the further direction.

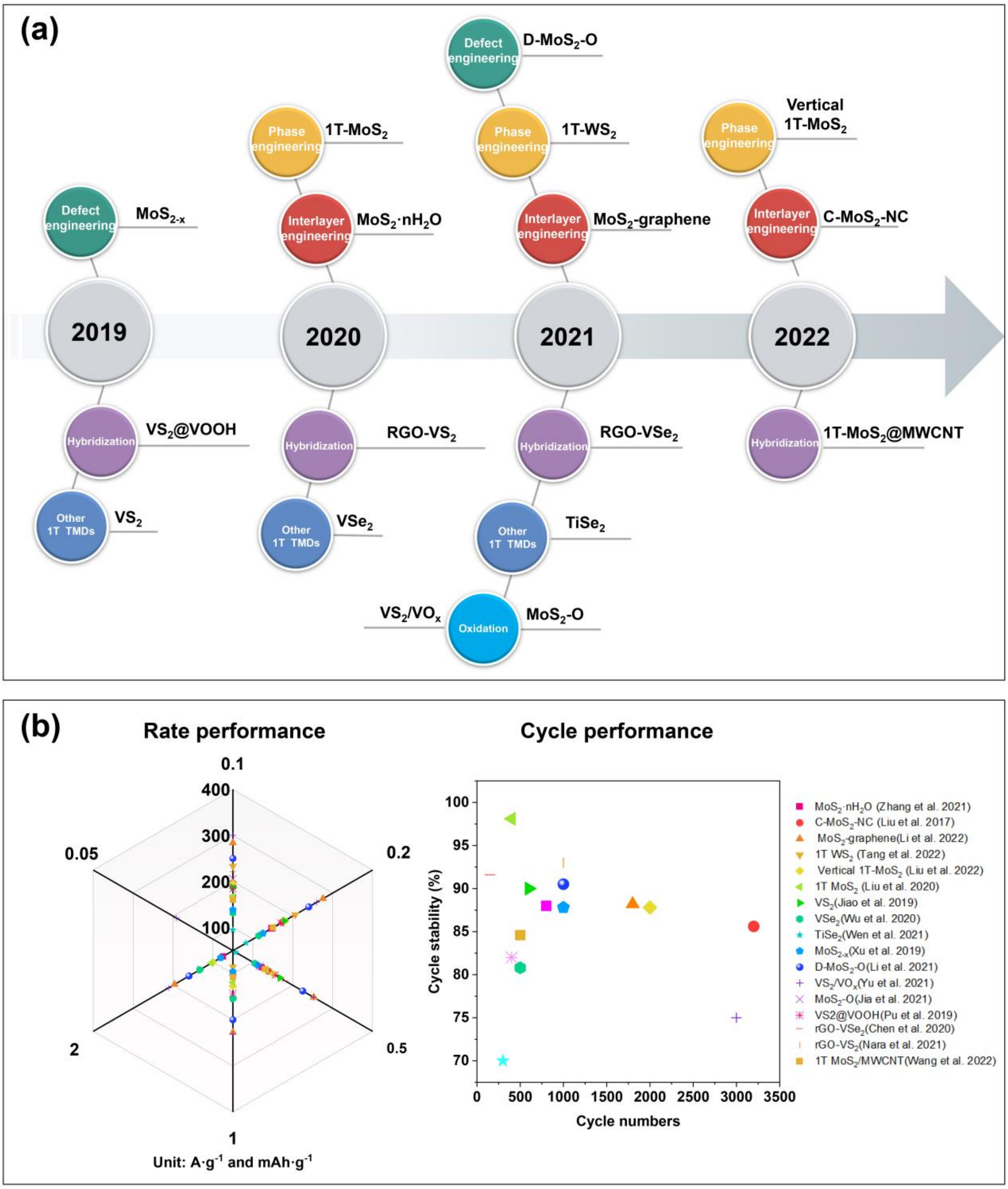

Figure 8. Summary of modified TMDs for high−performance ZIBs. (**a**) Timeline of developed strategies for TMD−based ZIB cathode. (**b**) The radar chart of the electrochemical performance of TMD materials as ZIB cathode. Refs. [12,14,16–18,22,23,28,29,42–44,47,51,54,55].

Table 1. Summary of the electrochemical performance of TMDs as ZIB cathode.

Strategies	Cathode Material	Electrolyte	Voltage	Capacity [mAh·g^{-1}]	Cycle Stability	Ref
Interlayer engineering	$MoS_2 \cdot nH_2O$	3M Zn $(CF_3SO_3)_2$	0.2–1.25 V	165 at 0.1 A g^{-1}	88% after 800 cycles at 2.0 A g $^{-1}$	[22]
	MoS_2−graphene	3M Zn $(CF_3SO_3)_2$	0.2–1.5 V	283.9 at 0.1 A g^{-1}	88.6% after 1800 cycles at 1.0 A g^{-1}	[12]
	C−MoS_2−NC	2 M $ZnCl_2$	0.2 to 1.4 V	247 at 0.1 A g^{-1}	85.6% after 3200 cycles at 1.0 A g^{-1}	[23]
Phase engineering	1T−MoS_2	3M Zn $(CF_3SO_3)_2$	0.25–1.25 V	168 at 0.1 A g^{-1}	98.1% after 400 cycles at 1.0 A g^{-1}	[14]
	1T−WS_2	1M $ZnSO_4$	0.1–1.5 V	206 at 0.1 A g^{-1}	/	[29]
	Vertical 1T−MoS_2	3M Zn $(CF_3SO_3)_2$	0.25–1.25 V	198 at 0.1 A g^{-1}	87.8% after 2000 cycles at 1.0 A g^{-1}	[28]
Defect engineering	MoS_{2-x}	3M Zn $(CF_3SO_3)_2$	0.25–1.25 V	138 at 0.1 A g^{-1}	87.8% after 1000 cycles at 1.0 A g^{-1}	[42]
	D−MoS_2−O	3M Zn $(CF_3SO_3)_2$	0.2–1.25 V	261 at 0.1 A g^{-1}	90.5% after 1000 cycles at 1.0 A g^{-1}	[15]
Metallic 1T	VS_2	1M $ZnSO_4$	0.4–1.0 V	159 at 0.1 A g^{-1}	98% after 200 cycles at 1.0 A g^{-1}	[43]
	VSe_2	2M $ZnSO_4$	0.1–1.6 V	132 at 0.1 A g^{-1}	80.8% after 500 cycles at 1.0 A g^{-1}	[44]
	$TiSe_2$	2M $ZnSO_4$	0.05–0.6 V	128 at 0.2 A g^{-1}	70% after 300 cycles at 1.0 A g^{-1}	[16]
Oxidation	VS_2/VO_x	25M $ZnCl_2$	0.1–1.8 V	260 at 0.1 A g^{-1}	75% after 3000 cycles at 1.0 A g^{-1}	[47]
	MoS_2−O	3M Zn $(CF_3SO_3)_2$	0.2–1.3 V	206 at 0.1 A g^{-1}	/	[17]
Hybridization	VS_2@VOOH	3M Zn $(CF_3SO_3)_2$	0.4–1.0 V	165 at 0.1 A g^{-1}	86% after 200 cycles at 1.0 A g^{-1}	[51]
	rGO−VS_2	3M Zn $(CF_3SO_3)_2$	0.4–1.7 V	238 at 0.1 A g^{-1}	93% after 1000 cycles at 1.0 A g^{-1}	[54]
	rGO−VSe_2	2 M $ZnSO_4$	0.4–1.7 V	221at 0.1 A g^{-1}	91.6% after 150 cycles at 1.0 A g^{-1}	[18]
	1T−MoS_2−CNT	2 M $ZnSO_4$	0.2–1.3 V	161.5at 0.1 A g^{-1}	84.6% after 500 cycles at 1.0 A g^{-1}	[55]

Funding: This research received no external funding.

Institutional Review Board Statement: Not applicable.

Informed Consent Statement: Not applicable.

Data Availability Statement: All collected data are presented in the manuscript.

Conflicts of Interest: The author declares no conflict of interest.

References

1. Larcher, D.; Tarascon, J.-M. Towards greener and more sustainable batteries for electrical energy storage. *Nat. Chem.* **2015**, *7*, 19–29. [CrossRef] [PubMed]
2. Tang, W.; Zhu, Y.; Hou, Y.; Liu, L.; Wu, Y.; Loh, K.P.; Zhang, H.; Zhu, K. Aqueous rechargeable lithium batteries as an energy storage system of superfast charging. *Energy Environ. Sci.* **2013**, *6*, 2093–2104. [CrossRef]
3. Jia, X.; Liu, C.; Neale, Z.G.; Yang, J.; Cao, G. Active materials for aqueous zinc ion batteries: Synthesis, crystal structure, morphology, and electrochemistry. *Chem. Rev.* **2020**, *120*, 7795–7866. [CrossRef] [PubMed]

4. Liang, G.; Mo, F.; Ji, X.; Zhi, C. Non-metallic charge carriers for aqueous batteries. *Nat. Rev. Mater.* **2021**, *6*, 109–123. [CrossRef]
5. Liang, G.; Zhu, J.; Yan, B.; Li, Q.; Chen, A.; Chen, Z.; Wang, X.; Xiong, B.; Fan, J.; Xu, J. Gradient fluorinated alloy to enable highly reversible Zn-metal anode chemistry. *Energy Environ. Sci.* **2022**, *15*, 1086–1096. [CrossRef]
6. Ding, J.; Gao, H.; Ji, D.; Zhao, K.; Wang, S.; Cheng, F. Vanadium-based cathodes for aqueous zinc-ion batteries: From crystal structures, diffusion channels to storage mechanisms. *J. Mater. Chem. A* **2021**, *9*, 5258–5275. [CrossRef]
7. Zhang, T.; Tang, Y.; Fang, G.; Zhang, C.; Zhang, H.; Guo, X.; Cao, X.; Zhou, J.; Pan, A.; Liang, S. Electrochemical activation of manganese-based cathode in aqueous zinc-ion electrolyte. *Adv. Funct. Mater.* **2020**, *30*, 2002711. [CrossRef]
8. Cao, T.; Zhang, F.; Chen, M.; Shao, T.; Li, Z.; Xu, Q.; Cheng, D.; Liu, H.; Xia, Y. Cubic Manganese Potassium Hexacyanoferrate Regulated by Controlling of the Water and Defects as a High-Capacity and Stable Cathode Material for Rechargeable Aqueous Zinc-Ion Batteries. *ACS Appl. Mater. Interfaces* **2021**, *13*, 26924–26935. [CrossRef]
9. Du, W.; Ang, E.H.; Yang, Y.; Zhang, Y.; Ye, M.; Li, C.C. Challenges in the material and structural design of zinc anode towards high-performance aqueous zinc-ion batteries. *Energy Environ. Sci.* **2020**, *13*, 3330–3360. [CrossRef]
10. Li, T.; Li, H.; Yuan, J.; Xia, Y.; Liu, Y.; Sun, A. Recent Advance and Modification Strategies of Transition Metal Dichalcogenides (TMDs) in Aqueous Zinc Ion Batteries. *Materials* **2022**, *15*, 2654. [CrossRef]
11. Lee, W.S.V.; Xiong, T.; Wang, X.; Xue, J. Unraveling MoS_2 and Transition Metal Dichalcogenides as Functional Zinc-Ion Battery Cathode: A Perspective. *Small Methods* **2021**, *5*, 2000815. [CrossRef] [PubMed]
12. Liu, W.; Hao, J.; Xu, C.; Mou, J.; Dong, L.; Jiang, F.; Kang, Z.; Wu, J.; Jiang, B.; Kang, F. Investigation of zinc ion storage of transition metal oxides, sulfides, and borides in zinc ion battery systems. *Chem. Commun.* **2017**, *53*, 6872–6874. [CrossRef] [PubMed]
13. Li, S.; Liu, Y.; Zhao, X.; Shen, Q.; Zhao, W.; Tan, Q.; Zhang, N.; Li, P.; Jiao, L.; Qu, X. Sandwich-Like Heterostructures of MoS_2/Graphene with Enlarged Interlayer Spacing and Enhanced Hydrophilicity as High-Performance Cathodes for Aqueous Zinc-Ion Batteries. *Adv. Mater.* **2021**, *33*, 2007480. [CrossRef]
14. Liu, J.; Xu, P.; Liang, J.; Liu, H.; Peng, W.; Li, Y.; Zhang, F.; Fan, X. Boosting aqueous zinc-ion storage in MoS_2 via controllable phase. *Chem. Eng. J.* **2020**, *389*, 124405. [CrossRef]
15. Li, S.; Liu, Y.; Zhao, X.; Cui, K.; Shen, Q.; Li, P.; Qu, X.; Jiao, L. Molecular Engineering on MoS_2 Enables Large Interlayers and Unlocked Basal Planes for High-Performance Aqueous Zn-Ion Storage. *Angew. Chem.* **2021**, *133*, 20448–20455. [CrossRef]
16. Wen, L.; Wu, Y.; Wang, S.; Shi, J.; Zhang, Q.; Zhao, B.; Wang, Q.; Zhu, C.; Liu, Z.; Zheng, Y. A Novel $TiSe_2$ (De) Intercalation Type Anode for Aqueous Zinc-Based Energy Storage. *Nano Energy* **2021**, *93*, 106896. [CrossRef]
17. Jia, H.; Qiu, M.; Tawiah, B.; Liu, H.; Fu, S. Interlayer-expanded MoS_2 hybrid nanospheres with superior zinc storage behavior. *Compos. Commun.* **2021**, *27*, 100841. [CrossRef]
18. Narayanasamy, M.; Hu, L.; Kirubasankar, B.; Liu, Z.; Angaiah, S.; Yan, C. Nanohybrid engineering of the vertically confined marigold structure of rGO-VSe_2 as an advanced cathode material for aqueous zinc-ion battery. *J. Alloys Compd.* **2021**, *882*, 160704. [CrossRef]
19. Liu, B.; Du, J.; Yu, H.; Hong, M.; Kang, Z.; Zhang, Z.; Zhang, Y. The coupling effect characterization for van der Waals structures based on transition metal dichalcogenides. *Nano Res.* **2021**, *14*, 1734–1751. [CrossRef]
20. Wang, Q.H.; Kalantar-Zadeh, K.; Kis, A.; Coleman, J.N.; Strano, M.S. Electronics and optoelectronics of two-dimensional transition metal dichalcogenides. *Nat. Nanotechnol.* **2012**, *7*, 699–712. [CrossRef]
21. Liang, H.; Cao, Z.; Ming, F.; Zhang, W.; Anjum, D.H.; Cui, Y.; Cavallo, L.; Alshareef, H.N. Aqueous zinc-ion storage in MoS_2 by tuning the intercalation energy. *Nano Lett.* **2019**, *19*, 3199–3206. [CrossRef] [PubMed]
22. Zhang, Z.; Li, W.; Wang, R.; Li, H.; Yan, J.; Jin, Q.; Feng, P.; Wang, K.; Jiang, K. Crystal water assisting MoS_2 nanoflowers for reversible zinc storage. *J. Alloys Compd.* **2021**, *872*, 159599. [CrossRef]
23. Li, C.; Liu, C.; Wang, Y.; Lu, Y.; Zhu, L.; Sun, T. Drastically-enlarged interlayer-spacing MoS_2 nanocages by inserted carbon motifs as high performance cathodes for aqueous zinc-ion batteries. *Energy Storage Mater.* **2022**, *49*, 144–152. [CrossRef]
24. Leng, K.; Chen, Z.; Zhao, X.; Tang, W.; Tian, B.; Nai, C.T.; Zhou, W.; Loh, K.P. Phase restructuring in transition metal dichalcogenides for highly stable energy storage. *ACS Nano* **2016**, *10*, 9208–9215. [CrossRef]
25. Voiry, D.; Mohite, A.; Chhowalla, M. Phase engineering of transition metal dichalcogenides. *Chem. Soc. Rev.* **2015**, *44*, 2702–2712. [CrossRef]
26. Fujita, T.; Ito, Y.; Tan, Y.; Yamaguchi, H.; Hojo, D.; Hirata, A.; Voiry, D.; Chhowalla, M.; Chen, M. Chemically exfoliated ReS_2 nanosheets. *Nanoscale* **2014**, *6*, 12458–12462. [CrossRef]
27. Zeng, Z.; Yin, Z.; Huang, X.; Li, H.; He, Q.; Lu, G.; Boey, F.; Zhang, H. Single-layer semiconducting nanosheets: High-yield preparation and device fabrication. *Angew. Chem.* **2011**, *123*, 11289–11293. [CrossRef]
28. Liu, J.; Gong, N.; Peng, W.; Li, Y.; Zhang, F.; Fan, X. Vertically aligned 1T phase MoS_2 nanosheet array for high-performance rechargeable aqueous Zn-ion batteries. *Chem. Eng. J.* **2022**, *428*, 130981. [CrossRef]
29. Tang, B.; Tian, N.; Jiang, J.; Li, Y.; Yang, J.; Zhu, Q. Investigation of zinc storage capacity of WS_2 nanosheets for rechargeable aqueous Zn-ion batteries. *J. Alloys Compd.* **2022**, *894*, 162391. [CrossRef]
30. Hu, Z.; Wu, Z.; Han, C.; He, J.; Ni, Z.; Chen, W. Two-dimensional transition metal dichalcogenides: Interface and defect engineering. *Chem. Soc. Rev.* **2018**, *47*, 3100–3128. [CrossRef]
31. Liang, G.; Gan, Z.; Wang, X.; Jin, X.; Xiong, B.; Zhang, X.; Chen, S.; Wang, Y.; He, H.; Zhi, C. Reconstructing Vanadium Oxide with Anisotropic Pathways for a Durable and Fast Aqueous K-Ion Battery. *ACS Nano* **2021**, *15*, 17717–17728. [CrossRef] [PubMed]

32. Zhang, X.; Liao, Q.; Liu, S.; Kang, Z.; Zhang, Z.; Du, J.; Li, F.; Zhang, S.; Xiao, J.; Liu, B. Poly(4-styrenesulfonate)-induced sulfur vacancy self-healing strategy for monolayer MoS_2 homojunction photodiode. *Nat. Commun.* **2017**, *8*, 15881. [CrossRef] [PubMed]
33. Zhang, X.; Liao, Q.; Kang, Z.; Liu, B.; Liu, X.; Ou, Y.; Xiao, J.; Du, J.; Liu, Y.; Gao, L. Hidden vacancy benefit in monolayer 2D semiconductors. *Adv. Mater.* **2021**, *33*, 2007051. [CrossRef]
34. Zhou, W.; Zou, X.; Najmaei, S.; Liu, Z.; Shi, Y.; Kong, J.; Lou, J.; Ajayan, P.M.; Yakobson, B.I.; Idrobo, J.-C. Intrinsic structural defects in monolayer molybdenum disulfide. *Nano Lett.* **2013**, *13*, 2615–2622. [CrossRef] [PubMed]
35. Li, H.; Tsai, C.; Koh, A.L.; Cai, L.; Contryman, A.W.; Fragapane, A.H.; Zhao, J.; Han, H.S.; Manoharan, H.C.; Abild-Pedersen, F. Activating and optimizing MoS_2 basal planes for hydrogen evolution through the formation of strained sulphur vacancies. *Nat. Mater.* **2016**, *15*, 48–53. [CrossRef] [PubMed]
36. Lin, Z.; Carvalho, B.R.; Kahn, E.; Lv, R.; Rao, R.; Terrones, H.; Pimenta, M.A.; Terrones, M. Defect Engineering of Two-Dimensional Transition Metal Dichalcogenides. *2D Mater.* **2016**, *3*, 022002. [CrossRef]
37. Chee, S.S.; Lee, W.J.; Jo, Y.R.; Cho, M.K.; Chun, D.; Baik, H.; Kim, B.J.; Yoon, M.H.; Lee, K.; Ham, M.H. Atomic vacancy control and elemental substitution in a monolayer molybdenum disulfide for high performance optoelectronic device arrays. *Adv. Funct. Mater.* **2020**, *30*, 1908147. [CrossRef]
38. Cai, Y.; Zhou, H.; Zhang, G.; Zhang, Y.-W. Modulating carrier density and transport properties of MoS_2 by organic molecular doping and defect engineering. *Chem. Mater.* **2016**, *28*, 8611–8621. [CrossRef]
39. Liu, D.; Guo, Y.; Fang, L.; Robertson, J. Sulfur vacancies in monolayer MoS_2 and its electrical contacts. *Appl. Phys. Lett.* **2013**, *103*, 183113. [CrossRef]
40. Koh, G.; Zhang, Y.-W.; Pan, H. First-principles study on hydrogen storage by graphitic carbon nitride nanotubes. *Int. J. Hydrogen Energy* **2012**, *37*, 4170–4178. [CrossRef]
41. Yao, K.; Xu, Z.; Huang, J.; Ma, M.; Fu, L.; Shen, X.; Li, J.; Fu, M. Bundled defect-rich MoS_2 for a high-rate and long-life sodium-ion battery: Achieving 3D diffusion of sodium ion by vacancies to improve kinetics. *Small* **2019**, *15*, 1805405. [CrossRef] [PubMed]
42. Xu, W.; Sun, C.; Zhao, K.; Cheng, X.; Rawal, S.; Xu, Y.; Wang, Y. Defect engineering activating (Boosting) zinc storage capacity of MoS_2. *Energy Storage Mater.* **2019**, *16*, 527–534. [CrossRef]
43. Jiao, T.; Yang, Q.; Wu, S.; Wang, Z.; Chen, D.; Shen, D.; Liu, B.; Cheng, J.; Li, H.; Ma, L. Binder-free hierarchical VS_2 electrodes for high-performance aqueous Zn ion batteries towards commercial level mass loading. *J. Mater. Chem. A* **2019**, *7*, 16330–16338. [CrossRef]
44. Wu, Z.; Lu, C.; Wang, Y.; Zhang, L.; Jiang, L.; Tian, W.; Cai, C.; Gu, Q.; Sun, Z.; Hu, L. Ultrathin VSe_2 Nanosheets with Fast Ion Diffusion and Robust Structural Stability for Rechargeable Zinc-Ion Battery Cathode. *Small* **2020**, *16*, 2000698. [CrossRef] [PubMed]
45. Luo, H.; Wang, B.; Wang, F.; Yang, J.; Wu, F.; Ning, Y.; Zhou, Y.; Wang, D.; Liu, H.; Dou, S. Anodic oxidation strategy toward structure-optimized V_2O_3 cathode via electrolyte regulation for Zn-ion storage. *ACS Nano* **2020**, *14*, 7328–7337. [CrossRef]
46. Cao, Z.; Chu, H.; Zhang, H.; Ge, Y.; Clemente, R.; Dong, P.; Wang, L.; Shen, J.; Ye, M.; Ajayan, P.M. An in situ electrochemical oxidation strategy for formation of nanogrid-shaped $V_3O_7 \cdot H_2O$ with enhanced zinc storage properties. *J. Mater. Chem. A* **2019**, *7*, 25262–25267. [CrossRef]
47. Yu, D.; Wei, Z.; Zhang, X.; Zeng, Y.; Wang, C.; Chen, G.; Shen, Z.X.; Du, F. Boosting Zn^{2+} and $NH_4{}^+$ Storage in Aqueous Media via In-Situ Electrochemical Induced VS_2/VO_x Heterostructures. *Adv. Funct. Mater.* **2021**, *31*, 2008743. [CrossRef]
48. Tan, C.; Zhang, H. Two-dimensional transition metal dichalcogenide nanosheet-based composites. *Chem. Soc. Rev.* **2015**, *44*, 2713–2731. [CrossRef]
49. Lu, Q.; Yu, Y.; Ma, Q.; Chen, B.; Zhang, H. 2D transition-metal-dichalcogenide-nanosheet-based composites for photocatalytic and electrocatalytic hydrogen evolution reactions. *Adv. Mater.* **2016**, *28*, 1917–1933. [CrossRef]
50. Yang, J.; Zhu, J.; Xu, J.; Zhang, C.; Liu, T. $MoSe_2$ Nanosheet Array with Layered MoS_2 Heterostructures for Superior Hydrogen Evolution and Lithium Storage Performance. *ACS Appl. Mater. Interfaces* **2017**, *9*, 44550–44559. [CrossRef]
51. Pu, X.; Song, T.; Tang, L.; Tao, Y.; Cao, T.; Xu, Q.; Liu, H.; Wang, Y.; Xia, Y. Rose-like vanadium disulfide coated by hydrophilic hydroxyvanadium oxide with improved electrochemical performance as cathode material for aqueous zinc-ion batteries. *J. Power Sources* **2019**, *437*, 226917. [CrossRef]
52. Kumar, N.A.; Dar, M.A.; Gul, R.; Baek, J.-B. Graphene and molybdenum disulfide hybrids: Synthesis and applications. *Mater. Today* **2015**, *18*, 286–298. [CrossRef]
53. Chen, D.; Tang, L.; Li, J. Graphene-based materials in electrochemistry. *Chem. Soc. Rev.* **2010**, *39*, 3157–3180. [CrossRef] [PubMed]
54. Chen, T.; Zhu, X.; Chen, X.; Zhang, Q.; Li, Y.; Peng, W.; Zhang, F.; Fan, X. VS_2 nanosheets vertically grown on graphene as high-performance cathodes for aqueous zinc-ion batteries. *J. Power Sources* **2020**, *477*, 228652. [CrossRef]
55. Wang, Y.-T.; Zhang, Z.-Z.; Li, M. One-pot synthesis of 1T MoS_2/MWCNT hybrids for enhanced zinc-ion storage. *Nano Futures* **2022**, *6*, 025001. [CrossRef]